Simulation of Optical Properties of the $Si/SiO_2/Al$ Interface at the Rear of Industrially Fabricated Si Solar Cells

Yang Yang[1,**] and Pietro P. Altermatt[1,2,*]
[1]Institute for Solar Energy Research Hamelin (ISFH), Emmerthal, Germany
[2]Dep. Solar Energy Research, Inst. Solid-State Physics, Leibniz University of Hanover, Germany
*Corresponding author: Appelstr. 2, 30167 Hanover, Germany, altermatt@solar.uni-hannover.de
**On leave from Institute for Solar Energy Systems, Sun Yat-Sen University, Guangzhou, China

Abstract: The specular and diffuse reflection properties of sunlight at the rear surface of silicon solar cells with various degrees of roughness are computed by solving the Maxwell and material equations in two dimensions, using the COMSOL RF MODULE. The model is first tested on planar Si/SiO_2/air interfaces, where perfect agreement with the Fresnel theory is attained within numerical precision. The chosen simulation domain is similar to typical experimental scattering measurements. A simulation with planar $Si/SiO_2/Al$ interfaces confirms an angular resolution of the specular beam of about 10°, and a lower resolution limit for scattering probability near 10^{-3}. The simulations show that for wavelength of 800 nm, (i) maximum scattering is achieved with a standard deviation for roughness between 50 nmand 100 nm, (ii) the distribution probabilities for scattering are similar (but restricted to certain scattering angles) if roughness is produced by etching solely the grown SiO_2 instead of the Si. Output parameters for geometrical ray tracers are computed.

Keywords: Silicon solar cells, scattering, diffuse reflection, roughness, aluminum, SiO_2

1. Introduction

In this paper, geometrical structures are theoretically investigated on a nanometer scale to improve the optical properties of the rear surface of Si solar cells. Silicon has a relatively low absorption coefficient. Therefore, the amount of photo-generation in Si solar cells depends crucially on the light trapping scheme [1]: the front surface of the cells is commonly textured with random pyramids by means of KOH etching. The size of the pyramids depends on the etching conditions and ideally does only weakly influence the effectiveness of light trapping. Usually, pyramids with a base length of about 10 μm are etched, because etching considerably smaller pyramids tends to reduce the fractional area between pyramids and (near) planar regions. For these reasons, the classic pyramidal texturing often cannot be applied to thin Si cells [2].

An issue is the trade-off between improved optical properties and deteriorated electrical properties: the pyramidal surface has a higher area than a planar surface, causing more recombination of photo-generated electron-hole pairs before they reach the external contacts. Usually, the power output efficiency improves with texturing because optical improvements dominate the electrical losses. However, there is room for improvement of the electrical properties.

For the above geometric and electric reasons, there is a large demand to develop "flat" texturing schemes. In fact, it is sufficient to merely scatter the incoming rays at the rear surface (or both surfaces), instead of deflecting them.

Scattering is accomplished by geometric features with the size smaller than the wavelength of the light. In this paper, we solve the Maxwell equations to model the optical properties of surfaces that have been roughened in a random way. As far as we are aware, the first numerical solutions of the Maxwell equations at randomly rough surfaces were published in 1978 [3] using the method of moments (also called the boundary element method). This method is not often used anymore because the matrix is fully populated. In subsequent years, computing capacity increased such that more elaborated models became feasible. For example, finite-difference time-domain (FDTD) simulations at rough surfaces were reported in two dimensions in 1991 [4] and in three dimensions in 1994 [5]. These simulations usually require a dual tensor grid to solve the E- and the H fields, respectively. In this paper, we solve the Maxwell and materials

equations in two dimensions with the finite-element simulator COMSOL, using the RF MODULE. The matrices are only banded, which saves both computer capacity and CPU time when applying recently emerged solvers like UMFPACK and Pardiso. Also, the mesh consists of triangles, which keeps the number of grid points to a minimum near the randomly rough surface. We investigate the impact of roughness on the angular distribution of diffuse reflection. Initially, we test the model at planar surfaces by comparing the results with analytic calculations.

Traditionally, the rear surface of Si cells is fully covered with an aluminum layer, leading to parasitic absorption at the rear surface, i.e. at the rear interface between Si and Al. It is well known that the reflection at the rear surface can be substantially improved by, firstly, growing a SiO_2 layer and, subsequently, placing the Al layer on top of that oxide. Such a planar $Si/SiO_2/Al$ structure is included in some designs of solar cells. Roughening this structure may significantly improve the light trapping properties of such cells.

2. Numerical model

We use the RF MODULE of COMSOL version 3.4 to solve the Maxwell equations,

$$\begin{aligned} \frac{\partial \vec{B}}{\partial t} &= -\nabla \times \vec{E} \qquad \nabla \cdot \vec{D} = \rho \\ \frac{\partial \vec{D}}{\partial t} &= \nabla \times \vec{H} - \vec{J} \qquad \nabla \cdot \vec{B} = 0 \end{aligned} \tag{1a}$$

and material equations,

$$\vec{D} = \varepsilon \vec{E} \qquad \vec{B} = \mu \vec{H} \qquad \vec{J} = \sigma \vec{E} \ . \tag{1b}$$

The symbols have their usual meaning. Combining these equations results in

$$\mu \frac{\partial \vec{H}}{\partial t} = -\nabla \times \vec{E} \qquad \frac{\partial \varepsilon \vec{E}}{\partial t} = \nabla \times \vec{H} - \sigma \vec{E} \ . \tag{2}$$

We express the electric and the magnetic fields by the vector potential $\vec{A}$:

$$\mu \vec{H} = \nabla \times \vec{A} \qquad \vec{E} = -\frac{\partial \vec{A}}{\partial t}, \tag{3}$$

and insert it into (2) to obtain

$$\mu_0 \sigma \frac{\partial \vec{A}}{\partial t} + \mu_0 \frac{\partial}{\partial t} \varepsilon \frac{\partial \vec{A}}{\partial t} + \nabla \times (\mu_0^{-1} \nabla \times \vec{A}) = 0 \ . \tag{4}$$

Our excitations are harmonic (planar waves), thus the response (i.e. scattered, reflected, and transmitted waves) will also be harmonic. Therefore, we factorize (4) in an amplitude- and a time-dependent factor:

$$\vec{E}(\vec{r},t) = \vec{E}(\vec{r}) e^{i\omega t} \qquad \vec{H}(\vec{r},t) = \vec{H}(\vec{r}) e^{i\omega t} \ . \tag{5}$$

We thus arrive at the well-known time-harmonic formulation:

$$\begin{aligned} \nabla \times (\mu^{-1} \nabla \times \vec{E}) - \omega^2 \varepsilon_c \vec{E} &= 0 \\ \nabla \times (\varepsilon_c^{-1} \nabla \times \vec{H}) - \omega^2 \mu \vec{H} &= 0 \end{aligned} \tag{6}$$

where ε_c is the complex permittivity:

$$\varepsilon_c = \varepsilon - i \frac{\sigma}{\omega} \ . \tag{7}$$

Although equations (6) appear to be independent of each other, they are interrelated by (1). We solve (6) with the UMFPACK or Pardiso solver after meshing the domain with triangles. When meshing, we choose as maximum element size one tenth of the wavelength λ of the generated radiation, as is done successfully in FDTD simulations. We take the material parameters for silicon from [6], for aluminum from [7], for SiO_2 and Ag from [8], using

$$\mathrm{Re}(\varepsilon) = n^2 - k^2 \qquad \mathrm{Im}(\varepsilon) = 2nk \ . \tag{8}$$

We do not need to enter σ into the model because there holds $\sigma = \omega \mathrm{Im}(\varepsilon)$ with ω given in (5); instead, we define a complex $\varepsilon = \mathrm{Re}(\varepsilon) + i\mathrm{Im}(\varepsilon)$. Since our simulations are in two dimensions, we scattering in the TM mode dominates scattering in the TE mode.

3. Simulations of planar surfaces

We test our model first at a planar interface structure. The simulation domain and a typical solution are shown in Fig. 1. At the left edge, a planar wave is generated at a port boundary condition. In Comsol's port boundary excitation feature, we define the oblique propagation angle α by

$$\begin{aligned} &k1x = k0\_emwh*n1*\cos(alpha), \\ &k1y = k0\_emwh*n1*\sin(alpha), \\ &H_{0z} = \exp(-i*k1y*y) \end{aligned} \qquad (9)$$

with n1 denoting the real part of the refractive index and k1x the propagation constant in region 1, etc. See the Comsol RF guide for the definition of k0_emwh.

The wave then travels towards the planar interface. At the upper and lower edges of the domain, we use the Floquet boundary condition:

$$H_{dest} = H_{source}\exp(-ik\cdot(r_{dest} - r_{source})) \; . \qquad (10)$$

The boundary condition ensures that a wave, when reaching the bottom edge (source), is transposed to the upper edge (destination) with the appropriate phase shift. With such periodic boundary conditions in the modeling domain, one has to take care not to introduce artificial effects caused by a diffracting grating with the period of the modeling domain. This is important, because sunlight has a lateral coherence length of about 70 µm [9].

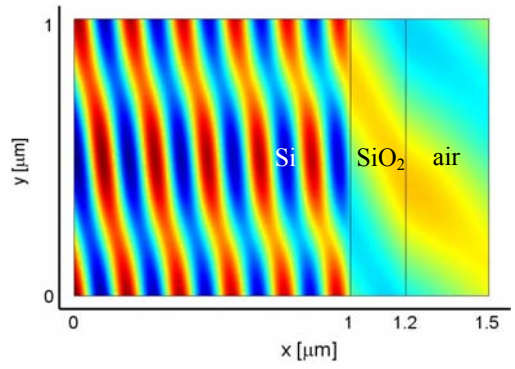

Figure 1. Domain for testing the simulation model at the rear surface of Si solar cells. A planar wave with vacuum wavelength λ = 800 nm is generated at the left edge at an oblique angle. Reflection at the 200 nm thick oxide causes a standing wave pattern. Colors: absolute E-Feld (TE mode).

At the interface, the waves get refracted according to Snell's law. This needs to be considered in the Floquet boundary conditions in the second medium:

$$\begin{aligned} &k2x = k0\_emwh*n2*\cos(alpha2) \\ &n1*\sin(alpha) = n2*\sin(alpha2) \end{aligned} \qquad (11)$$

The boundary condition of the right edge is also a port boundary condition but without excitation to ensure complete absorption of the incoming waves.

We compute the reflectance as follows: First, a background field model in which all layers are defined as Si is solved and the power outflow (obtained by the boundary integration method) at the interface is taken as incident power P_i. Then, the Si/SiO_2/Al model is solved and the power outflow at the interface is taken as transmitted power P_t. The reflectance at the interface then is $R = 1 - P_t/P_i$.

In Figure 2, we compare our simulation results at a planar Si/SiO_2/Al structure (where the air in Fig. 1 is replaced by Al) with analytical calculations [10] using the transfer matrix method based on the Fresnel equations. Perfect agreement is obtained within the small numerical tolerances.

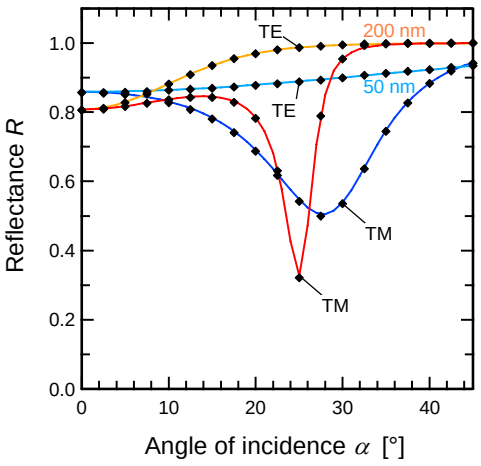

Figure 2. Simulated (lines) and calculated (symbols) reflectance at the planar Si/SiO_2/Al structure with an oxide thickness of 50 nm or 200 nm, respectively, as a function of the angle of incidence. The simulation domain is shown in Fig. 1. The simulation results agree perfectly with the analytical theory [10] within numerical tolerances. The wavelength λ of the incident wave is 800 nm.

4. Simulations of roughened surfaces

4.1 Definition of random surface

Surface roughness can be mathematically modeled in various ways. Figure 3 shows our approach. We choose an equidistant set of defining points in the y-direction with distance Δy, and a random set of x-values with normal (Gaussian) distribution defined by the standard deviation σ_{dev}. Adding a normal distribution to Δy influences the simulation results only marginally (as long as $\sigma_{dev} << \lambda$). For simplicity, we connect these points with straight lines to define the rough surface. Smooth Bezier curves would represent reality better in most cases, however our tests showed clearly that Bezier curves influence the simulation results again only marginally, as long as $\Delta y << \lambda$.

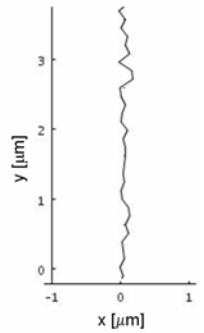

Figure 3. An example of a rough interface, generated with the SCRIPT module.

4.2 Choice of simulation domain

The simulation domain shown in Fig. 1 is unsuitable for extracting the angular distribution of scattered waves. Instead, we use the domain depicted in Fig. 4, which resembles experimental measuring set-ups. The beam of planar waves is generated at an average distance r_{beam} near the rough interface in order to minimize diffraction effects at the edge of the beam. The rough surface section extends well beyond the beam diameter d. This has the disadvantage that also the diffracted parts of the beam interact with the interface, but a smaller random domain would cause an overestimation of specular reflection. The scattered waves travel towards the circular edge at distance r_{edge} from the center of the interface. The edge consists of segments with angular width of 5º, so we can detect the outflowing energy with this angular resolution by means of the boundary integration feature during the postprocessing. All the edges are of scattering type, to absorb (or generate) the waves.

From Fig. 4 it becomes intuitively clear that an optimum set of r_{beam}, d, and r_{edge} must be chosen such as to

1. minimize the errors in the angular distribution of the scattered waves;
2. minimize artificial effects due to the diffracted edge of the beam;
3. minimize the "shadowing" of the detectors at the edge due to the beam generation;
4. keep the number of mesh points, i.e. the required RAM as well as CPU time, to a manageable size.

Presently, we use r_{edge} = 20 μm, d = 3 μm, and r_{beam} =5 μm.

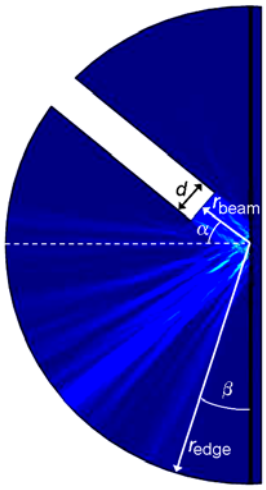

Figure 4. The domain used for simulating scattering at the rough interface. A beam (with diameter d) of plane waves impinges on the interface at incident angle α. The scattered waves are detected at multiple sections of the edge of the domain, such that the angular (β) distribution of scattering can be extracted. Colors: energy density (absolute Poynting vector).

The beam diameter d ideally must be rather large to achieve both (i) a reduced relative amount of diffraction at the edge of the ray, and (ii) illumination of many interface segments (having width Δy) to obtain well averaged statistical results. However, a large d requires also a large r_{edge} (and hence a large mesh) to preserve the angular resolution of the scattering

signal. We choose a compromise by setting d small enough so the signal from the diffracted beam parts does not limit the precision too much, and we obtain a well averaged statistics of the scattering intensities by repeating the simulations with randomly changed surfaces (per chosen σ_{dev}) ten to twenty times.

4.3 Choice of the wavelength

The choice of the defining parameters for roughness, Δy and σ_{dev}, depend on the wavelength λ, because scattering phenomena scale with λ. The thicker the cell, the longer is λ of sunlight that penetrates to the rear surface. The cells under consideration in this work are about 30 μm thick, where λ = 800 nm is the lower limit. We present our results at this shortest wavelength, as this poses the highest demand on the mesh – remembering that the mesh resolution should be at least about one tenth of λ.

4.4 Extraction of the optical parameters

We compute the angularly resolved reflectance as follows. The boundary integration feature of Comsol delivers the outgoing energy flux density in units of W/m at the circular edge segments, while the generated flux in the linear segment is given in units of W/m as well. A direct comparison of these two values does not render the *integrated* reflectance R, because there is absorption within the silicon. The most direct way to arrive at the integrated reflectance, with minimal influence from numerical tolerances, turned out to be the following. We simulate first a planar structure. Integration (summation) over all segments in the circular edge yields I_{planar} in units of W. We multiply this value with a constant a such that the R obtained from Fig. 2 equals $R = aI_{planar}$. Then, we simulate rough interfaces, and multiply their energy fluxes by the same factor a because r_{edge} stays the same. The values in each segment (the angularly resolved reflectivites) then have also the meaning of scattering probabilities.

The simulation results will mainly be used as an input for a geometrical ray tracing software. There, each photon is traced along its pass. At every interaction event at an optical boundary, the simulator decides randomly with a Monte Carlo algorithm, whether the photon is

1. reflected, transmitted or absorbed,
2. whether reflection/transmission occurs in a specular or diffuse way, and
3. if diffuse, in which direction the photon continues.

We need to statistically weight the first decision with the integrated R, the transmittance T, and the absorbance A, dependent on incident angle. For the second decision, we need the fraction between specular and diffuse reflection or transmission, while for the third decision we need a probability distribution of scattering angles. These values are extracted from the simulation results shown in Figs. 5 and 6.

5. Discussion of results

Figure 5 shows the simulated probabilities as a function of angle β (defined in Fig. 4) for two different structures:

(a) a rough Si surface, where the oxide is grown, and subsequently Al is evaporated; and
(b) a planar Si surface, where the grown oxide is partly etched back, before Al is evaporated.

While in case (a) both interfaces are rough (and parallel), only the SiO_2/Al interface is rough in case (b). Due to Al, $T = 0$, and only the reflection properties are shown. Also, we only show the results obtained with an angle of incidence α = 20°, while the roughness is defined with equidistance Δy = 125 nm.

5.1 Resolution/precision of simulations

The planar surface (black curve) indicates the angular resolution and precision of the simulation method. The angular resolution of the specular reflection is about 10°. The diffracted edge of the incoming beam limits the lower limit of scattering probability to about 10^{-3} in a decreasing manner away from the specular beam. This quality is sufficient for generating input to a geometrical ray tracer; it may be improved by adjusting the simulation domain. Note that we linearly interpolate the values in the "shadow" of the light source, i.e. between β of 95° and 130°. The fluctuations within neighboring segments give an impression of how well the signal is statistically averaged; 10 simulations turn out to be sufficient for probabilities down to 5×10^{-4}.

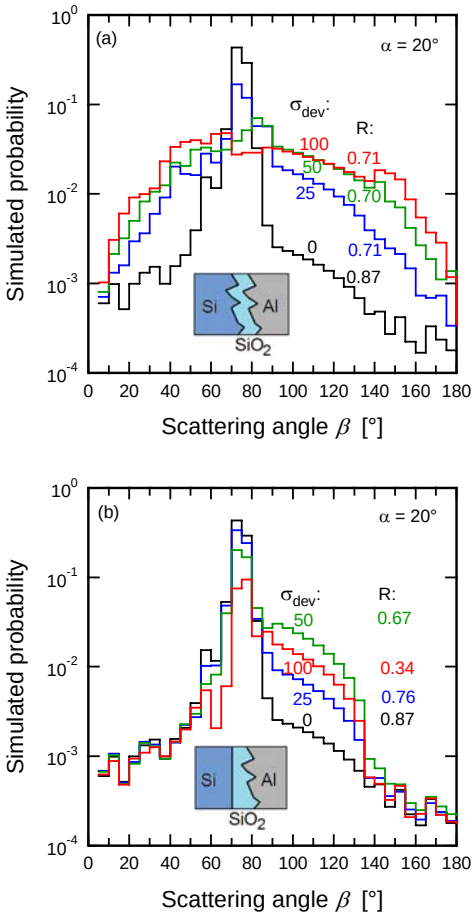

Figure 5 (top and bottom). The simulated scattering probability as a function of incident angle β (in segments of 5°) for the case of two different interface structures shown in the insets. Labels indicate the standard deviation of roughness, σ_{dev}, and the reflectance R (integrated over all angles, including the specular beam).

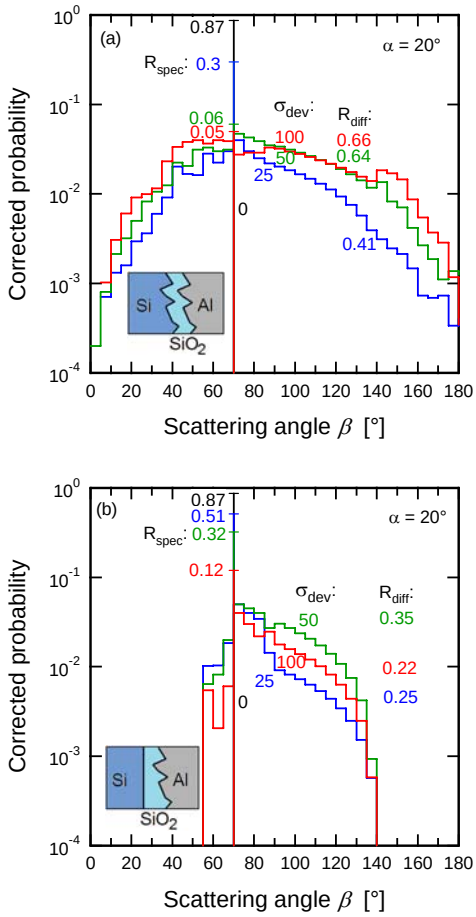

Figure 6 (top and bottom). The same as in Fig. 5, but corrected for input in optical ray tracing. The total R of Fig. 5 is divided in a specular part, R_{spec}, and a diffuse part R_{diff}.

5.2 Scattering properties

The colored lines in Fig. 5 indicate the results obtained with various degrees of roughness as labeled.

Surfaces with a standard deviation $\sigma_{dev} < 25$ nm cause lass than 10% scattering and fall close to our present detection limit.

From σ_{dev} of 25 nm to 50 nm, the angular scattering probabilities increase in a congruent way, while the integrated R (including the specular reflection) decreases slightly as labeled. A similar angular distribution is reported in Ref. 4. Interestingly, a $\sigma_{dev} > 50$ nm reduces the angular probabilities, because there is an increased amount of interaction with the aluminum, leading to more absorption; this strongly reduces the integrated R (including the specular reflection). The important implication is that an optimum σ_{dev} exists near 50 nm for diffuse reflection, but whether this is beneficial to light trapping depends sensitively on the amount of specular reflection as well and must be decided with a ray tracer.

The structure (b) with a planar Si/SiO_2 interface causes scattering only to a limited range of angles β. All scattered rays reflect from the

rough SiO_2/Al interface and must penetrate back into Si, where they get refracted. SiO_2 has a considerably lower refractive index than Si. Hence, rays entering Si from a parallel angle in respect to the smooth Si/SiO_2-interface have $\beta \approx 50°$ or 135°, respectively. Thus, there is no scattering below $\beta \approx 50°$ and above 135°, and the signals of the various σ_{dev} values coincide within the statistical limit (which reduces with the number of simulations per σ_{dev} value).

Interestingly, the angular scattering probabilities of structure (b) are very similar to structure (a), just condensed in respect to the angle β. Whether this condensation reduces the effectiveness of light trapping will be decided by means of ray tracing. At σ_{dev} = 25 nm, structure (b) has higher values of R than structure (a), and may be more beneficial for light trapping despite its condensed scattering angles. The optimum values of σ_{dev}, seem to be different among the two structures.

5.3 Scattering probabilities for ray tracer

In order to render input values for the geometric ray tracer, the data shown in Fig. 5 must be processed as shown in Fig 6. Because our angular distribution is discretized in steps of 5°, we divide the probabilities in specular R_{spec} and diffuse parts R_{diff}. With this, the specular part is treated by the ray tracer by the exact Snell's law, but with a lower reflectivity than would be obtained with the Fresnel equations alone (due to the scattering part). This procedure avoids discretization errors to appear in ray tracing. The diffuse part needs to be corrected in those parts where its probabilities approach the detection limit (given by the black curves obtained with the planar structure). This can be easily done at far angles δ from the specularly reflected beam, as for example in the second structure. However, at close angles, care must be taken, because these scattering parts are completely dominated by the angular resolution of the specular reflection. This problem has also been addressed in Ref. [4]. Fortunately, in light trapping schemes, small angular deviations from specular reflection are by far not as significant as for example in ray tracing for image processing, where glows around light sources appear. Hence, we presently extrapolate from larger to smaller angles of δ.

6. Conclusions

A COMSOL model for the angular distribution of scattering at rough interfaces is established, having an angular resolution of the specular beam of about 10°, and a lower detection limit for scattering probability near 10^{-3}. A simulation example shows that optimal diffuse reflection is achieved with a standard deviation for roughness of about 50 nm.

8. References

[1] P. Campbell and M. A. Green, "Light trapping properties of pyramidally textured surfaces", *J. Applied Physics* **62**, 243 – 249 (1987).

[2] R. Brendel, *Thin-Film Crystalline Silicon Solar Cells*, Wiley-VCH, Weinheim, Germany, (2003).

[3] R. M. Axline and A K Fung, "Numerical computation of scattering from a perfectly conducting random surface", *IEEE Trans. on Antennas and Prop.* **26(3)**, 482 – 488 (1978).

[4] C. H. Chan, S. H. Lou, L. Tsang and J. A. Kong, "Electromagnetic scattering of waves by random rough surface: a finite-difference time-domain approach", *Microwave and Optical Technology Letters* **4(9)**, 355 – 359 (1991).

[5] A. K. Fung, M. R. Shah, and S. Tjuatja, "Numerical Simulation of Scattering from Three-Dimensional Randomly Rough Surfaces", *IEEE Transactions on Geoscience and remote sensing* **32(5)**, 986 – 994 (1994).

[6] M.A. Green, M. Keevers, "Optical properties of intrinsic silicon at 300 K", *Progress in Photovoltaics* **3**, 189 – 192 (1995).

[7] E. Shiles, T. Sasaki, M. Inokuti, and D. Y. Smith, "Self-consistency and sum-rule tests in the Kramers-Kronig analysis of optical data: applications to aluminum", *Physical Review B* **22(4)**, 1612 – 1628 (1980).

[8] D. E. Palik, "Handbook of optical constants of solids", Academic Press, Boston, MS, (1985).

[9] D. A. Gregory and G. Peng, "Random faced Fresnel lenses and mirrors", *Optical Engineering* **40**, 713 – 719 (2001).

[10] B. Harbecke, "Coherent and incoherent reflection and transmission of multilayer structures", *Applied Physics* **B 39**, 165 – 170 (1986).